MESO-SCALE MODELS FOR THE INTERACTION OF DAMAGE MODES IN COMPOSITES LAMINATES

S. Ghiasvand[1], A. Airoldi[1], G. Sala[1], P. Aceti[1], P. Ballarin[1], A. Baldi[2], E. Mesiani[2]

[1] Dept. of Aerospace Science and Technology, Politecnico di Milano,
alessandro.airoldi@polimi.it
[2] Leonardo Helicopters Division, Leonardo Company

Abstract: The response of complex composite parts for primary aeronautical structures, such as rotorcraft rotors, is influenced by the evolution of different damage modes. The numerical analysis of such phenomena has been undertaken within a joint project of Politecnico di Milano and Leonardo Helicopter. The approach consists of a ply-wise bi-phasic FE model of the laminate that makes possible a representation of both delamination and intralaminar matrix damage within the elements representing an idealized matrix phase. Accordingly, the coupling between intralaminar cracks and delamination can be introduced in the matrix constitutive law, without requiring meshes refined at the sub-ply level. The theoretical aspects of the approach are summarized and attention is focused on a series of application cases, to illustrate the effectiveness of the technique. In particular the interaction between transverse matrix-cracking and delamination are analysed, considering tensile coupons of glass-reinforced fabric and the response of curved laminates with a cross-ply lay-up is studied. The results indicates the potential of the approach for the prediction of the loads required to nucleate and propagate damages in real-world structural elements with complex geometry and lay-ups.

Keywords: Bi-phasic approach, Transverse damage, Delamination, Interaction, Fracture

INTRODUCTION

Fiber/resin composite material attracts designers due to the need of reducing the structural weight and improve performance. As all the fibres in composite laminates are in one plane, at least in the elements manufactured by the well-assessed lamination technique, the material naturally behaves differently considering the properties in the planes where fibres lay and in the directions perpendicular to such plane. Indeed, lamination of long fibre reinforced plies means that the most appealing structural properties are also in the same plane [1]. Based on this condition, the mechanical properties of the in-plane direction are significantly higher than through the thickness direction. This feature strengthens the composite against planar stresses and makes it weaker for out-of-plane stresses. As a matter of fact, impact and out-of-plane stresses (known as interlaminar stress) are the leading cause of failure in composite components.

Besides all the advantages of using advanced composite material to produce lightweight and strong structures, some aspects still limit the designer from using the maximum potential of this material. One

of the most critical parameters in composite material is the detection of defects and damages. Undetected defects and damages directly affect the residual strength of composite specimens [2]. Therefore, the high-accuracy analysis method is necessary to study the complex failure processes involving intra- and inter-laminar damage in composite laminates.

The damage simulation can be a combination of different scales and approaches based on the damage modes. Delamination is basically stimulated by approaches based on LEFM, like Virtual Crack Closure Technique (VCCT) or Cohesive Zone Models (CZM). VCCT is a well-known approach for computing the energy release rate and predicting the propagation of the crack; however, the crack needs to be pre-existed, and its location must be defined in advance. The CZM has the possibility to predict the initiation and propagation of the crack even in the case that the location of the crack is not known. These approaches are more convenient in modeling discrete damages like delamination or debonding. Interface damages are often modelled by individual cracks by embedding cohesive elements in the interface under study [3-6]. Most of the study on delamination is based on the DCB test [7, 8] and the methods adopted can be extended to adhesive interface between composite adherents, as in Mall et al. [9]. Bi-linear and exponential cohesive failure are the most common method in cohesive modelling, but more complex laws can be adopted, as in Airoldi and Davila [10], where a trilinear cohesive law is adopted to simulate fibre bridging in unidirectional S2/Cyron SP250 glass-reinforced DCB specimens.

For the interlaminar damage, the most common approach is Continuum Damage Mechanics (CDM). This approach can model initiation and propagation of the transverse matrix cracking and the consequent degradation of stiffness in case of damage. The method can be applied at the scale of the ply or even at the sub-ply level [11, 12]. Many studies have been performed to represent inelastic mechanisms in orthotropic composites by exploiting the effect of several scalar damage variables, to simulate the degradation of the transverse and in-plane shear moduli and the Poisson's ratios [13-23]. These activities continue the work performed by Laws and Dvorak [24-26] and Hashin [27].

The study of individual transverse matrix cracks has been carried out in different approaches, which typically involves a statistical distribution of properties. Bailey et al. [28-32] studied the progressive development of transverse cracks between already existing cracks. Manders et al. [33] and Fukunaga et al. [34] used the Weibull distribution of strength in the ply under study. In comparison, Wang and Crossman [35] use the distribution of flaw sizes and locations to predict laminate damage behaviour. Laws and Dvorak [36] used the energy-based criteria that a transverse crack occurs when the opening energy meets its defined value.

Although transverse matrix damage is not catastrophic, it triggers other damage modes like delamination [37-42]. Furthermore, matrix cracks with sharp edges can be like stress raisers that cause failure in adjacent plies [43]. Several studies tried to demonstrate the correct interaction behaviour of damagesAccurate simulations needs microscale modeling with at least ten elements in the thickness direction of each ply [21, 40, 44]. To decrease the computational and modelling effort, the scale must be changed to mesoscale so to study the damage behaviour as a ply scale. For this reason, the material's properties need to be calibrated appropriately [45]. Iarve [46] used XFEM in the mesoscale to simulate damage interaction. In some studies, the cohesive elements are implemented both transversally and longitudinally between elements to represent the transverse and delamination, relying on the model capability to capture interactions even with meso-scale meshes [42, 45, 47]. Abisset et al. [22] use a non-local finite element procedure where the interlaminar parameter depends on the intralaminar damage of adjacent layers. Mohammadi et al. [48] used a similar approach by substituting the elements with high-order shell elements to capture the 3D stress state of integration points through the thickness.

A particular numerical approach for modelling different types of damages is the bi-phasic approach proposed by Airoldi et al. [49, 52], which is based on the division of the matrix and fibre phase of the composite with the possibility of direct interaction between damage modes. In this study, the application of such an approach to capture transverse cracking interaction with delamination in cross-ply specimens and angular elements, as it will be described in the following sections.

BI-PHASIC NUMERICAL APPROACH WITH COHESIVE ZONE MODELS

Fundamental aspects of the modelling technique

The approach followed in this work moves from the results obtained in [49, 52] and is based on a bi-phasic decomposition of the properties in a long fibre reinforced composite ply, which is carried out to distinguish the stiffness contribution originated by the continuity of the reinforcement from the ones that are mainly influenced by the properties of the resin and the characteristic of resin-fibre interaction. Such a decomposition, represented in Figure 1-A, produces two idealized material phases, which can be characterized by different constitutive laws: a fibre phase carrying only stress in the reinforcement direction and an effective medium representing the matrix-dominated response of the laminate. In the elastic range, the bi-phasic constitutive law is represented in Eqn. 1.

$$\begin{bmatrix}\sigma_{11}\\ \sigma_{22}\\ \sigma_{33}\\ \tau_{12}\\ \tau_{23}\\ \tau_{31}\end{bmatrix} = \left(\begin{bmatrix} E^{f-eff}V_f & 0 & 0 & 0 & 0 & 0 \\ 0 & 0 & 0 & 0 & 0 & 0 \\ 0 & 0 & 0 & 0 & 0 & 0 \\ 0 & 0 & 0 & 0 & 0 & 0 \\ 0 & 0 & 0 & 0 & 0 & 0 \\ 0 & 0 & 0 & 0 & 0 & 0 \end{bmatrix} + \begin{bmatrix} D_{11}^m & D_{12}^m & D_{13}^m & 0 & 0 & 0 \\ D_{21}^m & D_{22}^m & D_{23}^m & 0 & 0 & 0 \\ D_{31}^m & D_{32}^m & D_{33}^m & 0 & 0 & 0 \\ 0 & 0 & 0 & D_{44}^m & 0 & 0 \\ 0 & 0 & 0 & 0 & D_{55}^m & 0 \\ 0 & 0 & 0 & 0 & 0 & D_{66}^m \end{bmatrix} \right) \begin{bmatrix}\varepsilon_{11}\\ \varepsilon_{22}\\ \varepsilon_{33}\\ \gamma_{12}\\ \gamma_{23}\\ \gamma_{31}\end{bmatrix} \quad (1)$$

Where E^{f-eff} is an effective modulus that describe the contribution of the reinforcement continuity and V_f the volumetric fraction of the fibers. Methods for the identification of E^{f-eff} have been presented in [50], for a decomposition of the in-plane stiffness properties, and in [49] for a full three-dimensional decomposition. Such methods are aimed to obtain both a realistic representation of the stiffness provided by the fibres in the reinforcement directions and a physically admissible material representing the effective medium of the matrix phase.

In the application of the approach proposed in [49, 52], these idealized phases are used to characterized two types of elements. The composite laminates is seen as a lay-up of membrane elements with the properties of the fibre phase, oriented in the proper direction and lumped at the mean plane of the physical plies, embedded in a matrix phase represented by solid elements, which connect the fibre phase elements. The resulting technique is represented in Figure 1-B.

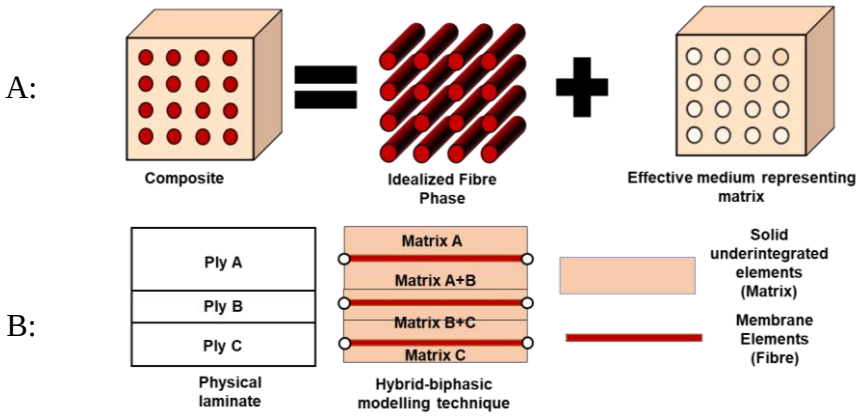

Figure 1: Bi-phasic decomposition (A) and hybrid modelling technique applied to a laminate (B).

The technique should not be considered a micromechanical approach, since the idealized phases are not directly related to physical materials and, moreover, their constitutive laws are formulated in terms of the same average strain state in whole composites, as expressed in Eqn. 1.

A fundamental aspect of this unconventional technique is that the idealized matrix phase can be characterized to represent, within a single constitutive law, both the damages occurring in the resin and at the resin-fibre interface within the plies, that is intralaminar damage, which evolves in transverse matrix cracking, and the interlaminar damage developing at the interfaces between two adjacent plies, which evolve into delamination. To accomplish such objective, cohesive zone models (CZM) are

embedded in the solid element representing the idealized matrix phase, which connect the membrane elements representing the fibre phase lumped at the mid-plane of the plies. This approach makes possible simulating transverse cracking and delamination within the same element without requiring zero-thickness interface elements (cohesive elements). Such elements are nowadays available in most non-linear Finite Element codes, but are required to be extremely stiff before crack propagation, thus leading to computational disadvantages.

In previous works, the bi-phasic decomposition and the hybrid modelling schemes were separately assessed, such as in [50,51] and the two aspects of the approach were merged in [49, 52] to exploit the full potential of the technique, thus allowing to outline a series of important advantages with respect to more conventional meso-scale modelling approaches based on solid element, representing the plies, connected by cohesive elements. Beyond the advantages regarding computational costs (see [49, 51], two points are particularly important for the activities presented in this work:

- individual matrix cracking with a mesh at the meso-scale level can be represented, as shown in [49], since the modelling technique attenuates significantly the confinement effect of adjacent plies with different fibre orientations, discussed in [45];
- the approach offers a unique point of view to model both interlaminar and intralaminar matrix damage in the same constitutive law, and to better control their interactions [49, 52];

Such aspects were exploited in the activities presented in this paper to model transverse matrix cracking and delamination developing, and interacting, in cross-ply laminates.

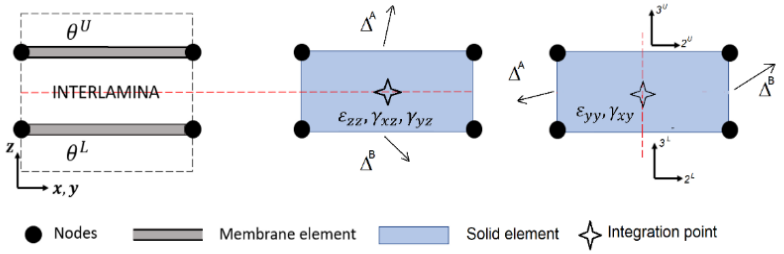

Figure 2: Role of the solid element representing the matrix phase and representation of discrete interlaminar and intralaminar fractures.

Two issues posed by the technique are represented by the need of applying a decomposition algorithm and by the difficulties involved in the hybrid meshing, though the latter are comparable to the ones related to the development of solid meshes connected by layers of cohesive elements. A more critical issue is represented by the fact that matrix elements actually represent the matrix phases of two adjacent plies, as shown in Figure 1-B. Since the matrix phase is generally an orthotropic material that has to be oriented according to the ply orientation, the structure of its constitutive law was conceived to address such a problem by applying simple assumptions on the composition of in-plane and out of plane stress states in the two semi-phases referred to the adjacent plies that have to be represented (see [49]). For the sake of brevity the details of such a structure will be omitted. The role of the solid element representing the matrix phase is illustrated in Figure 2, where θ_U and θ_L are the angle of orientation, in the plane *x-y*, of the upper ply and of the lower ply whose mid-planes are connected by the matrix elements. The constitutive law of the matrix phase, including the CZM's that will be described in the following sub-section, was implemented in a Fortran Vumat.f subroutine, to be used within the Simulia/Abaqus Explicit code in quasi-static non-linear analyses.

Application of cohesive zone models to the idealized matrix phase

The constitutive law of the idealized matrix phase includes the application of CZM's to represent both delamination and matrix cracking in the solid elements. The CZM's, which are typically expressed as traction-separation laws at the interfaces and implemented in zero-thickness cohesive elements, are re-written in terms of stress-strain law to be included in 8-noded hexahedral solid elements with a reduced integration scheme, usually adopted in explicit FE analyses and characterized by a single integration

point at the centre of the element, as indicated in Figure 2. Cohesive elements model the process of fracture by using the discontinuities at the interface that they represent. Such discontinuities are defined by two vectors δ^A and δ^B, which are projected onto the directions of possible crack development to define the crack opening according to the different modes conventionally adopted in fracture mechanics: δ_I, δ_{II} and δ_{III}. The CZM's embedded in the matrix elements according to the approach presented, the fracture process is smeared in the volume of the element and the energy required to develop a crack is expressed considering the finite displacements (Δ_A and Δ_B) of the element faces, which are exemplified in Fig. 2 both for an interlaminar crack and an intralaminar crack in the matrix element. Assuming small displacements, the quantities, Δ_I, Δ_{II}, and Δ_{III}, which are used to describe a fracture within the element, can be related to the strain components at the central integration point of the element according to Eqn. 2, where the first set of equations is related to an interlaminar crack, while the second is referred to an intralaminar crack.

$$\begin{cases} \Delta_I = \Delta_z^A - \Delta_z^B = \varepsilon_{zz} l_{el} \\ \Delta_{II} = \Delta_x^A - \Delta_x^B = \gamma_{xz} l_{el} \\ \Delta_{III} = \Delta_y^A - \Delta_y^B = \gamma_{yz} l_{el} \end{cases} ; \quad \begin{cases} \Delta_I = \Delta_2^A - \Delta_2^B = \varepsilon_{22} l_{el} \\ \Delta_{II} = \Delta_1^A - \Delta_1^B = \gamma_{12} l_{el} \end{cases} \tag{2}$$

In Eqn. 2, l_{el} is the dimension of the element in the direction perpendicular to the crack, which plays the role of regularization parameter and is represented by the element thickness, for the interlaminar cracks, and by a typical element length in the plane of the plies, for the intralaminar cracks. The CZM for both the types of cracks is developed by defining a set of equivalent stress (σ_I, σ_{II}) and corresponding equivalent strains ($\varepsilon_I, \varepsilon_{II}$), which are related to the opening modes described in Eqn. (2). Damage variables are used to obtain the triangular response shown in Figure 3, which is typically adopted in CZM (see for instance [3,6, 53]). In this work, such a response is adopted both for stress-strain curves representing the interlaminar and the intralaminar response of the matrix idealized phase.

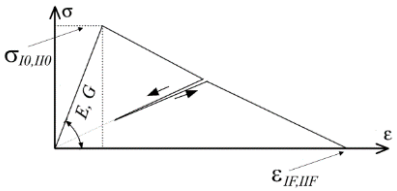

Figure 3: Typical bi-linear response adopted in CZM.

However, the definition of the equivalent stress and strain is different for intralaminar and interlaminar CZM model, as presented in Table 1. In both cases, the CZM makes possible controlling both the stress required for the onset of the crack ($\sigma_{I0}, \sigma_{II0}$ in Figure 3) and the energy required to completely degrade the matrix element, which is linked to the toughness of the fracture process through the relations in Eqn. 3. It is worth noting that the interlaminar process is defined in global axes, while the intralaminar process is described in material axis of each one of the semi-phases representing the matrix of adjacent plies and that both transverse cracks in the direction perpendicular to fibres (mode I) and shear cracks parallel to fibres (mode II) are described.

Table 1: Equivalent stress and strains for interlaminar and intralaminar CZM's.

	CZM for delamination	CZM for transverse cracking
Equivalent strain	$\varepsilon_I = \begin{cases} 0 & if\ \varepsilon_{zz} \le 0 \\ \varepsilon_{zz} & if\ \varepsilon_{zz} > 0 \end{cases}$ $\varepsilon_{II} = \sqrt{\gamma_{xz}^2 + \gamma_{yz}^2}$	$\varepsilon_I = \begin{cases} 0 & if\ \varepsilon_{22} \le 0 \\ \varepsilon_{22} & if\ \varepsilon_{22} > 0 \end{cases}$ $\varepsilon_{II} = \lvert\gamma_{12}\rvert$
Equivalent stress	$\sigma_I = \begin{cases} 0 & if\ \sigma_{zz} \le 0 \\ \sigma_{zz} & if\ \sigma_{zz} > 0 \end{cases}$ $\sigma_{II} = \sqrt{\tau_{xz}^2 + \tau_{yz}^2}$	$\sigma_I = \begin{cases} 0 & if\ \sigma_{22} \le 0 \\ \sigma_{22} & if\ \sigma_{22} > 0 \end{cases}$ $\sigma_{II} = \lvert\tau_{12}\rvert$

$$\begin{cases} G_{Ic} = \int_0^\infty \sigma_I d\Delta_I = l_{el} \int_0^\infty \sigma_I(\varepsilon_I) d\varepsilon_I \\ G_{IIc} = \int_0^\infty \sigma_{II} d\Delta_{II} = l_{el} \int_0^\infty \sigma_{II}(\varepsilon_{II}) d\varepsilon_{II} \end{cases} \quad (3)$$

According to the law described, three damage variables are included in the constitutive model attributed to the element of the idealized matrix phase: an out-of-plane matrix damage, d_{mo}, for delamination, and two damage variables to represent the transverse (or shear) cracking in the upper and lower semi-phases, d_{mc}^U and d_{mc}^L.

TRANSVERSE CRACKING AND DELAMINATION IN GLASS FIBER REINFORCED SPECIMENS

Experiments

Transverse matrix cracking is a significant benchmark for the investigation of interactions between interlaminar and intralaminar cracks since the mechanism of stress transmission from the cracked plies to the adjacent ones necessarily involves the development of interlaminar shear stress that can promote delaminations. Although several experimental activities have been conducted in the past ([25, 38-40, 44] to describe the phenomenon, it was decided to carry out specific tests on a S2-glass reinforced epoxy matrix, currently used in rotorcraft applications.

The results presented are referred to three tests performed on 250 mm long and 25 mm wide $[0/90_3/0]$ specimens, with a nominal cured ply thickness of 0.225 are hereby reported. Specimens were tested by using an MTS 858 systems. In a series of preliminary tests, the number of transverse cracks were evaluated both by using cellulose acetate replica and by back-illumination technique. However, the use of cellulose acetate replica was found to be more inaccurate and the necessary stops required during the tests influenced the acquisition of the force vs. displacement curves due to relaxation phenomena. Accordingly, the results hereby provided were obtained by analysing the images coming from the back-illumination technique, in test performed at a cross-head speed of 0.1 mm/min by using the set-up shown in Figure 4-A.

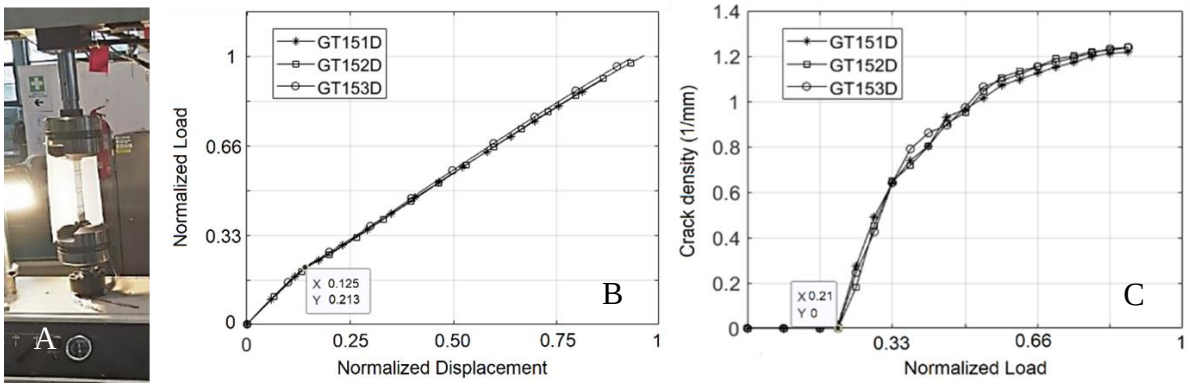

Figure 4: Set-up of tests on $[0/90_3/0]$ glass-reinforced specimens (A),force vs. displacement curves (B), and density of transverse cracks acquired through back-illumination technique (C)

The load vs. displacement curves and the crack density vs. load curves are reported in Figure 4-B,C. Loads and displacement are normalized with respect to the maximum values reached in the tests. It can be observed that the experiments present a very good repeatability. Transverse cracks appear at about 20% of the maximum load and induce an apparent knee in the force vs. displacement loads. The crack density increases linearly until a value of 0.8 crack per millimetre at one third of maximum load. The rate of crack growths starts decreasing and damage state tends to reach a saturation at about 1.2 crack per millimetre.

For the calibration of the material model, a series of tests were also performed on 250 mm long and 25 mm wide $[0]_5$ and $[90]_{10}$ specimens made of the same S2-glass reinforced material. Such tests were used

for the characterization of the elastic properties of the materials and for the evaluation of the tensile strength in the direction normal to the fibre reinforced, Y_T, which represent a basis for the calibration of a model capable to capture the transverse matrix cracking evolution. In the five tests performed on $[90]_{10}$ Y_T was identified with a coefficient of variance of about 8%.

Numerical model and calibration

Two types of the numerical model of a 1-element wide strip were developed by applying the hybrid-biphasic modelling technique that was previously presented. In the first one, represented in detail shown in Figure 5-A, the three central plies oriented at 90° are grouped in a single block. Hence, the model includes three membrane layers and four matrix elements, including a top and a bottom layers representing the matrix of the external 0-oriented plies. In the second, exemplified in Figure 5-B, each ply is separately modelled. This leads to five membrane elements and six solid elements.

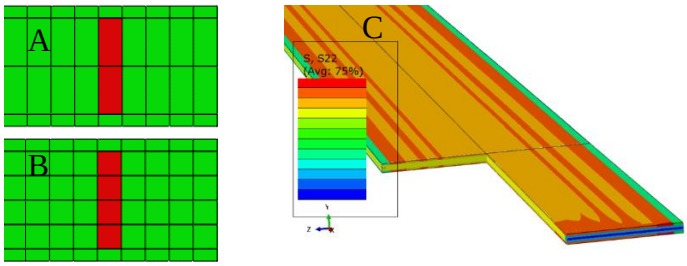

Figure 5: hybrid biphasic model with a 90_3 block plies treated as a single ply (A) and as three separate plies (B), and linear FE model to assess the thermal residual stress state (C).

A representation of the transverse matrix cracking evolution in a finite element model requires three fundamental ingredients, as it can be concluded from the analytical and numerical literature on the subject (see for instance [24-26, 33-34, 36, 39-40, 44-45]):

- the need of taking into account the role of thermal residual stress induced in the curing process of the composite;
- the consideration of the stress increment required to develop a crack due to the confinement effect of the adjacent plies with different fibre orientation, which oppose to the opening of the crack (*in-situ* effect);
- the statistical distribution of strength properties, which is the origin of the progressive increase of the density of cracks as the load increases.

The first aspect was considered by performing thermal stress analysis, simulating the cooling from 120°C to 20°C. Such step was carried out both for the strips modelled by using the hybrid-biphasic technique and, for confirmation, on a linear model representing the whole specimens with a ply-wise mesh consisting of conventional hexahedral elements. The Coefficient of Thermal Expansion, taken from [55], was set to 4.5 μm/m-°C in the fibre direction and 48.1 μm/m-°C in the transversal direction of the fibres.

The analyses confirmed the development of a significant tensile stress state in the *2*-axis direction of all the plies, as shown in Figure 5-C. In particular, for the group of the three central 90°-oriented ply, the σ_{22} stress reached more than 60% of the average Y_T value measured with the $[90]_{10}$ laminate with homogeneous lay-up. Analogous results were obtained on the one-element wide stripes.

For the *in-situ* effect, two theoretical models were applied ([36, 45]). The first one is considered valid for thin plies and introduces a link between the critical energy release rate associated with the fracture process in the direction transversal to the fibre, G_{Ic}, and thickness of the group of plies transversely oriented and the stress required to develop a crack $Y_{T-in\ situ}$, according to the formulation presented in Eqn. 4.

$$Y_{T-in\ situ} = \sqrt{\frac{8G_{Ic}}{\pi t \Lambda_{22}^0}} \quad ; \quad \Lambda_{22}^0 = 2\left(\frac{1}{E_{22}} - \frac{\nu_{21}^2}{E_{11}}\right) \tag{4}$$

According to this formulation very significant can be expected. For instance considering a G_{IC} of 0.5, the $Y_{T-in\ situ}$ is almost three time Y_T. The second approach was assessed for thick plies, and it consists of a fixed factor that amplifies the value obtained with homogeneous lay-up, as expressed in Eqn. 5

$$Y_{T-in\ situ} = 1.12\sqrt{2}Y_T \tag{5}$$

The formulation in Eq. 6 was applied considering different levels of G_{Ic}, which were chosen on the basis of the results provided in [10] for the interlaminar toughness of a very similar material. Finally, the statistic distribution of properties was included in the model, by applying both Gauss distributions, and Weibull distribution, following the approach presented in [45] and in [33]. Distribution were obtained by using the values of $Y_{T-in\ situ}$ as an average value and applying different standard deviation or different parameters for Weibull distributions.

Introduction of inter-intralaminar coupling and results

The model of the stripe developed at the ply level (see detail in Figure 5-B) was found more appropriate to capture the progression of crack density. A sensitivity study was carried out by varying the level of interlaminar toughness G_{Ic} to be used in Eqn. 6 and the parameters of the statistical distribution of properties. However, the results indicated that the tendency to saturation exhibited by the experiments could not be completely captured. As studied in [38-40], the modelling of such a response require the representation of the damage developed at the interfaces between the 0°-oriented and the 90°-oriented plies. Such interlaminar damage is triggered by the shear stress involved in the load transferring from the cracked 90°-oriented ply to the adjacent 0°-oriented ply, but the peak values of this interlaminar shear cannot be captured unless very fine meshes, with several element through the thickness of a ply, are adopted.

The modelling technique proposed in this work offers the opportunity of coupling interlaminar and intralaminar damage, thus allowing to mimic the presence of a transverse crack on the development of delamination without a detailed representation of the stress state below the meso-scale level. In the activity presented in this work, the coupling was obtained by reducing the strength and the toughness attributed to CZM of delamination in mode II as a function of the maximum between intralaminar damages, d_{mc}^U and d_{mc}^L, developed in the matrix semi-phases. As indicated in Eqn. 6, the coupling is modulated through a coefficient *h*, which can be varied between 0 and 1.

$$\begin{cases} \sigma'_{II0} = \sigma'_{II0}\left(1 - h \cdot max(d_{mc}^U, d_{mc}^L)\right) \\ G'_{IIc} = G'_{IIc}\left(1 - h \cdot max(d_{mc}^U, d_{mc}^L)\right) \end{cases} \tag{6}$$

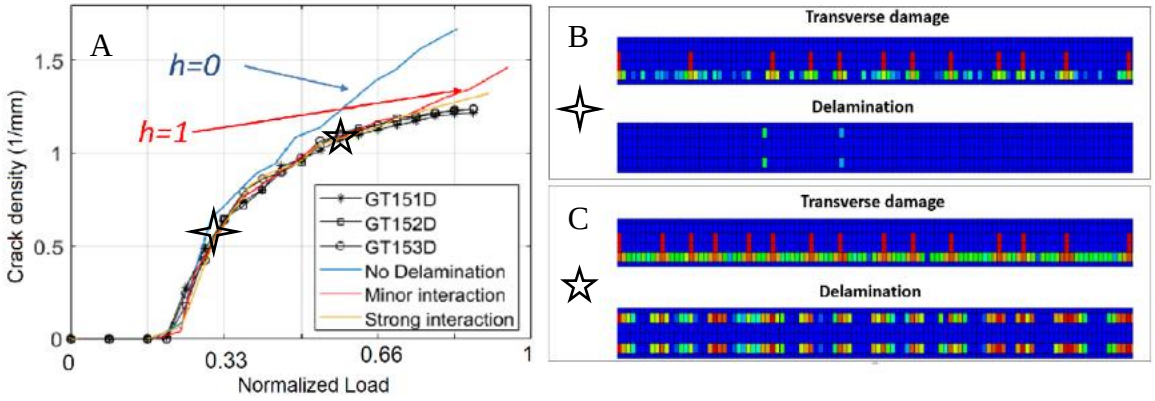

Figure 6 – Numerical-experimental correlation of crack density with and without inter-intralaminar coupling (A), contour of interlaminar and intralaminar damage at the onset of delamination (B) and with diffused delamination damage (C)

The results reported in Figure 6-A shows that, without any coupling, the crack density tends to growth with a slope significantly higher than in the experiments, while the application of coupling coefficient *h*=1 make possible a correct representation of the crack density progression. The contour of intralaminar and interlaminar damage in Figure 6-B is referred to the beginning of delamination onset, in the presence of a moderate crack density of transverse cracks, while the damage states at an higher load level is presented in Figure 6-C. All the presented analyses include a thermal step where a variation of temperature is applied to introduce the thermal residual stress in the analyses.

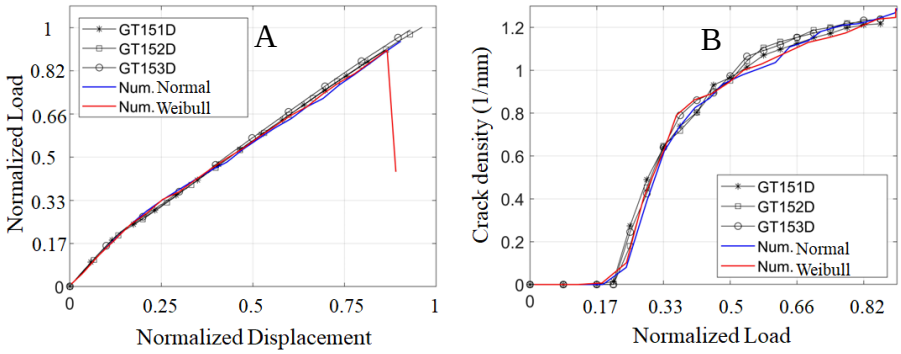

Figure 7: Numerical-experimental correlation of force vs. displacement (A) and crack density evolution (B) curves

The introduction of coupling made possible achieving an appreciable numerical experimental-correlation both at the level of crack density and for the forces vs. displacement results. Very good results can be achieved both by using a Gauss distribution and Weibull distribution, as shown in Figure 7. The main parameters of the CZM's for delamination (del) and transverse matrix cracking (TMC) adopted are presented in Table 2. It can be observed that a considerable in situ effect has to be considered and that a coefficient *h* of about 0.7 is required to correctly capture the tendency to saturation.

Table 2: Model parameters for best correlation

Distribution	$\frac{\sigma_{II0}-del}{Y_T}$	$G_{II}-del$ (KJ/mm^2)	$\frac{\sigma_{I0}-TMC}{Y_T}$	G_I-TMC (KJ/mm^2)	h *Coupling*
Normal	1.75	1.8	2.625 ± 0.325	0.5	0.68
Weibull	1.75	1.8	3.000 ± 0.200	0.5	0.68

INFLUENCE OF IN-PLANE DAMAGE ON DELAMINATION OF CURVED LAMINATES

Experimental activity

In a composite structure, sharply curved sections such as L- and C- shaped parts are among the most critical part in structural elements. Therefore, considering curved laminates, two lamination sequences of $[0]_{48}$ (Zero specimen) and $[0_2/90_2]_{6s}$ (Cross-ply specimen) were chosen for an experimental and numerical investigation on the pure delamination and the interaction between in-plane and out-of-plane stresses and damage modes. Three specimens of each lamination were produced by using CFRP unidirectional pre-preg with a vacuum bag technique.

Load application of the specimens was performed by an MTS 810 static tests system. The opening tension loading of specimens was applied by displacement control. The test set-up is reported in Figure 8-A. The specimen was tightly fixed by fixtures designed to grip a length of legs sufficient to avoid the specimen slipping during the test. Next, the specimen was connected to leave an adequate free span of 80 mm along the legs. This distance was measured from the end of the curvature to the fixture. For the connection of the fixture to MTS, a Y-shape fork transferred the loads from the MTS to the specimen by means of a 10 mm thick pin. The fixture was fixed in all directions except for the freedom of rotation

in the axis alongside the pin. This freedom of rotation allowed a correct transfer of forces to the center of the curved laminate.

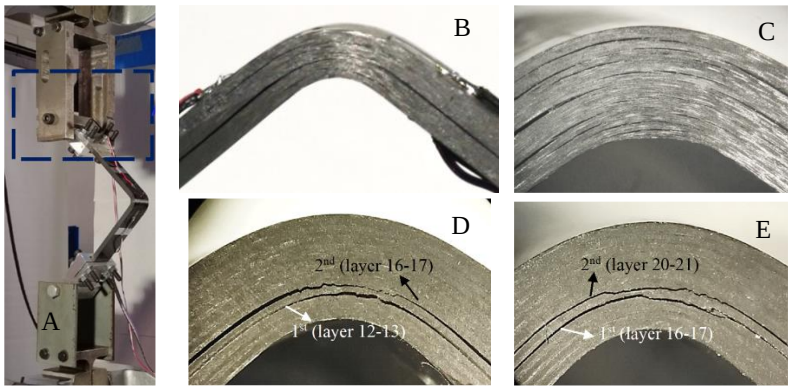

Figure 8- Set-up of experiments on angular specimens (A), failure mode in Zero specimens (B, C), and failure mode in Cross-ply specimens (D, E)

All of the Zero specimens had the same pattern of failure. After loading, one long delamination crack appeared at the one-third of the thickness direction from the inner, Figure 8-B,C. It was accompanied by multiple small delamination damages distributed all over the thickness direction. However, these cracks developed only in the curved area and did not go through the legs. All the cracks happened contemporarily. The Zero specimens experienced a catastrophic failure with losing all their load-carrying capability. The final shape of the Zero.S#3 specimen at the moment of failure during the test is shown in Figure 8-B,C.

Unlike Zero specimens, Cross-ply specimens did not lose all their strength at the first failure, so the test continued performing a second loading cycle. In the plots and results presented here, the first cycle of loading is defined by annotation "1st" and the second cycle of loading is indicated as "2nd". Each loading cycle continued until a clear drop of force in the force-displacement curve; then, the specimen is unloaded to capture the distortion of the specimen and start the next cycle. The damage at the moment of the first and second failure of Specimen CP.S#1 and CP.S#2 is shown in Figure 8-D,E. In all the specimens, one long crack appeared in the interface of [0/90] with at least one crack jump across the [90]2 to the upper or lower [0/90] interface. The crack jump involved a transverse matrix crack inside the $[90]_2$ layer.

Numerical model of Zero specimen:

The numerical model is following the bi-phasic approach. Each layer of composite is modeled by one element in the thickness direction to increase the accuracy of the modeling, Figure 9-A. Since the curved area is the stress concentration zone, the mesh in the curved area is denser than at the end of the legs.

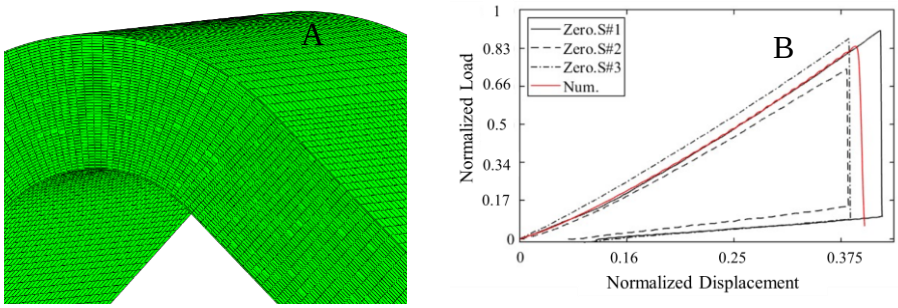

Figure 9 – Detail of the mesh developed according to hybrid-biphasic modelling technique (A) and numerical-experimental correlation for Zero specimen (B)

The correlation of numerical and experimental results of force versus displacement is plotted in Figure 9-B. The red curve shows the numerical results obtained by this modeling approach. Thanks to the realistic loading application, the non-linear behavior at the beginning of loading is also captured accurately. The correct detection of failure load indicates the proper assignment of interlaminar strength and toughness to the material. The numerical and experimental correlation of the load versus displacement curve indicates the correct assessment of the stiffness by the Bi-phasic approach.

The numerical model successfully captured the position of the main crack. One of the significant features of this modeling is the creation of multiple delaminations at once. Besides the main crack, which propagates through the leg, the other cracks are arrested in the curved area: experimental failure mode is correctly represented. As presented in Figure 10, the two sides of the specimen do not have the same pattern of damage, which means that oscillations in the solutions provided by the explicit time integration scheme introduce asymmetry despite the symmetry of initial boundary conditions. In the physical specimens, the asymmetrical behavior of crack generation and propagation can be attributed to the statistical distribution of property, the presence of defects, small asymmetry in load conditions captured by the asymmetry of the solution induced in numerical modeling. The specimen has view-cut to have a better vision on the inside of the numerical model. It is visible that the crack is not following the same interface for propagation through the width (direction 2), and they are limited in depth.

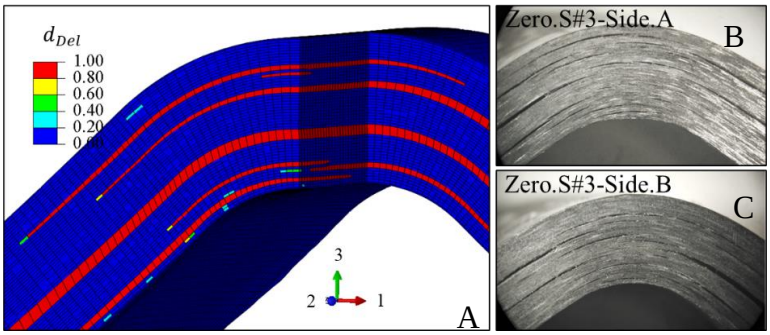

Figure 10 – Correlation of failure mode in Zero specimen: numerical results (A), damage scenario on both side of specimen #3 (B, C)

Introduction of intra-interlaminar coupling and modelling of Cross-ply specimen:

The same model of Zero specimen is used for the Cross-ply specimen by modifying the lay-up sequence. Since the delamination appears in the interfaces, the interlaminar damage model is activated in the matrix elements of [0/90] plies but is inhibited in the [90/90] and [0/0] matrix elements, that are at the interfaces of plies with identical orientation. Intralminar damage is activated in all the elements. The analysis for the Cross-ply specimen starts by performing a thermal stress analysis, simulating the cooling from 180°C to 20°C in the same way as mentioned in the previous section for the cross-ply tensile specimen. As shown in Figure 11, the amount of residual thermal stress is significantly high in 90˚ oriented layers of cross-ply specimen, almost reaching half of the Y_T of this material at the end of manufacturing. This high value of transverse stress indicates the possibility of a premature failure caused by transverse damage which eventually evolve in a delamination. To study this effect, the direct interaction between inter-intralaminar damage is implemented in the constitutive law.

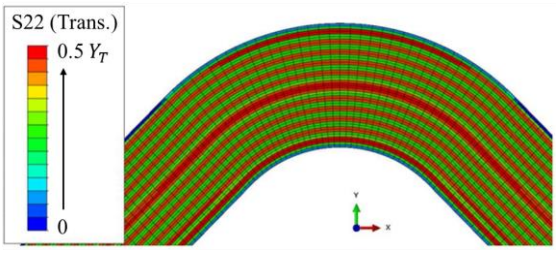

Figure 11- State of residual thermal stress in Cross-ply specimen at the end of manufacturing

A possible interpretation of the link between the scalar damage state in the bi-phasic approach and the evolution of a crack is shown in Figure 12. In this interpretation which follows the assumption of Laws and Dvorak [25,26], about the nucleation of transverse cracking in the core of the 90° oriented layers, the scale of transverse damage is related to the extension and to the opening of the transverse damaged area. In this sense, the damage is a scalar value that will be increased as the initial crack opening and extension is increased until a complete separation in the thickness. In the real material, the effect of the S33 stress incline the crack, and when the boundary of the layer is reached, a pure delamination is triggered; in the mesoscale model such a mechanism cannot be represented, but once the scalar damage reaches a certain threshold, the interlaminar properties can be modified so that delamination can be triggered at the interface.

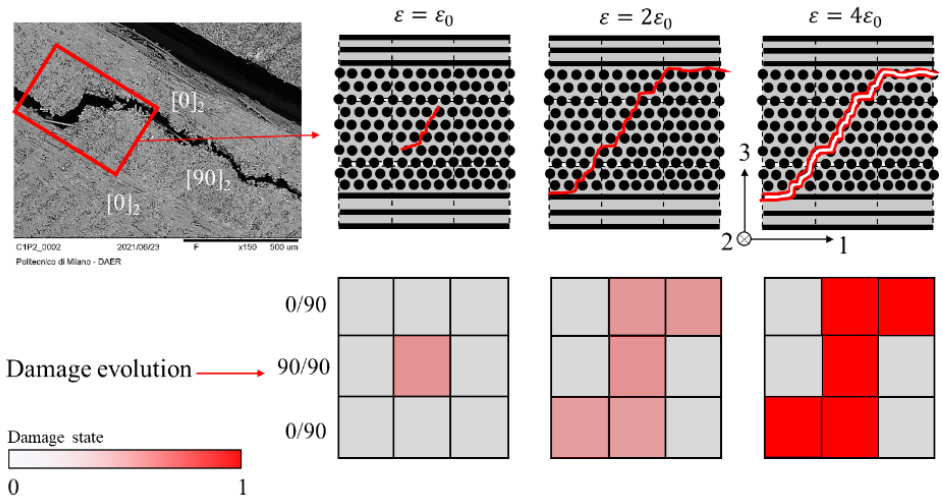

Figure 12 – Interpretation of the onset of delamination in Cross-ply specimens: experimental evidence, micro-scale idealization, and meso-scale representation

Accordingly, a direct interaction between intralaminar damage and ILTS value is established as shown in Figure 13-B. The load versus displacement curve of numerical results obtained by introducing such interaction between intralaminar damage and delamination are compared to the experimental results in Figure 13-A. The first load drop is captured accurately by numerical results; However, the second drop meets CP.S#1 and CP.S#2. This difference comes from the location of the first interface crack. In CP.S#1 and CP.S#2, the first crack appeared approximately one-third of the specimen's thickness from the inner radius, but in CP.S#3, the crack occurred in the middle of thickness. Therefore the numerical results correlate better with CP.S#1 and CP.S#2 than CP.S#3.

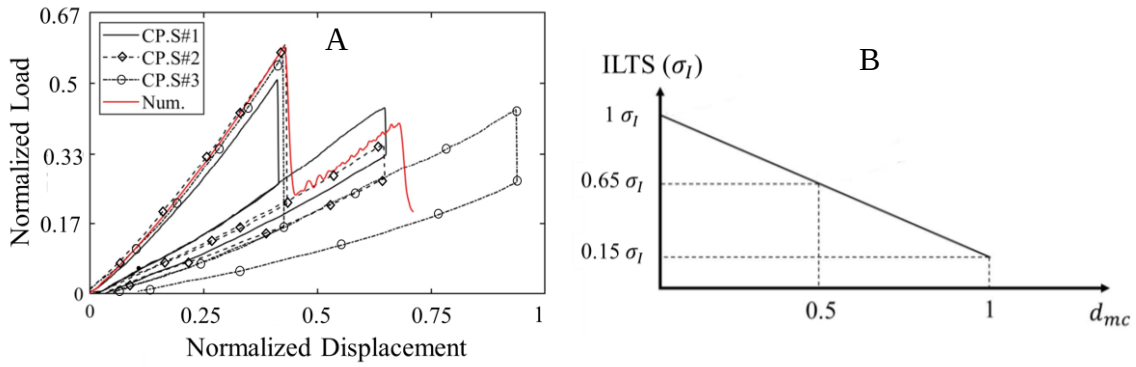

Figure 13 – Numerical-experimental correlation for Cross-ply specimen by adopting damage coupling: force vs. displacement curves (A) and interaction law between transverse damage and ILTS (B)

Figure 14 presents the numerical model of crack propagation of the Cross-ply specimen, considering the model where both the role of residual stress and the interaction between the incipient transverse

damage and the out-of-plane strength were introduced. The first interface crack that caused the first load drop appeared in the same displacement as in experimental tests. The delamination was sudden and propagated to the middle of the legs. By tracking the damage path from the middle to the legs, in the experiments CP.S#2 and CP.S#1, the crack migrated from the interface from the lower [0/90] (with respect to the inner radius) to the upper interface. This behaviour is also visible in numerical results. The main crack jumps that caused the crack migration, without crack branching, are precisely captured at the end of the bend, Figure 14-C. The state of the transverse crack at the moment of the first and second failure is shown in Figure 14-B,D. it can be observed that only at the location where crack jumps occur (white circles), the transverse damage reaches the unit value throughout the complete thickness of the 90° layers. Damage also reaches the unit value along the delamination path, which can also be interpreted considering the irregular path along the delamination. The minor transverse damages that cause the zig-zag pattern in the interface damage are shown by $d_{\text{transverse damage}}$= 0.6.

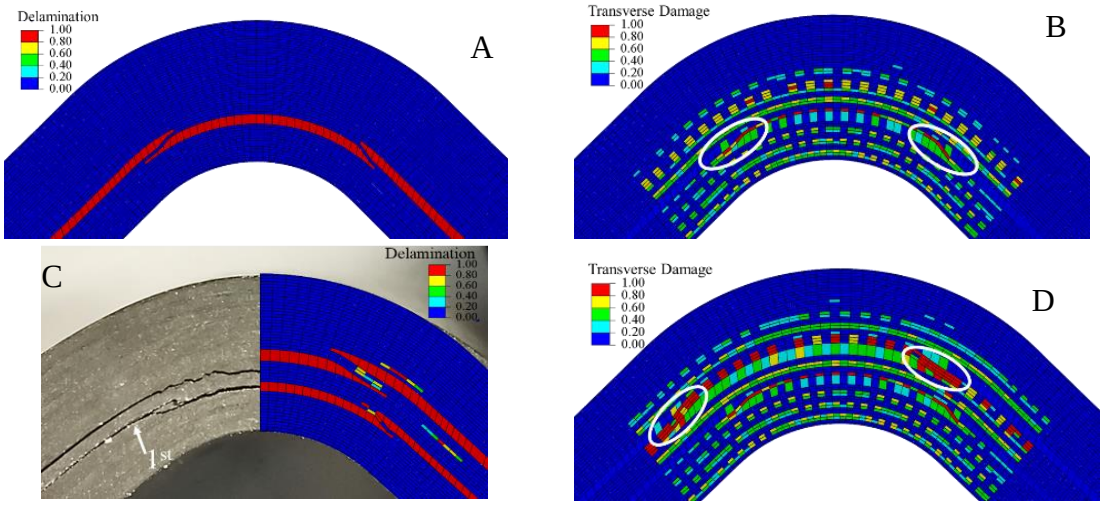

Figure 14 – Numerical delamination damage at first crack (A) and corresponding intralaminar damage (B), numerical-experimental correlation of delamination damage after second crack (C), and corresponding numerical intralaminar damage (D)

CONCLUSIONS

This activity aims to develop a high-fidelity numerical approach capable of modeling different damage modes and their interactions without requiring modelling at the sub-ply level. The bi-phasic approach proved an appealing method for developing efficient computational models to predict damage evolution without any prior estimation of the critical zones and to introduce simple interaction laws between inter-intralaminar mesoscale models without requiring a detailed representation of the stress fields at the micro-scale.

Two different interaction methods between inter-intralaminar were studied based on two case studies; tensile transverse crack test and opening of the curved specimen. In the first model, the interaction between transverse damage and mode II of out-of-plane damage correctly captured the rate of transverse damage density versus loading. In the second case study on the opening of the curved specimen, the interaction developed between transverse damage and ILTS value correctly captured the reduction of ILTS in the Cross-ply specimen, which led to an immature failure state compared to the Zero specimen. Furthermore, the activity results have shown the importance of modeling the residual stress state to develop a reliable prediction of damage evolution in real-world components.

REFERENCES

[1] Heslehurst, R.B. (2014), In: *Defects and damage in composite materials and structures*, CRC press Boca Raton.
[2] De Luca, A. and Caputo, F. (2017), *AIMS Mater. Sci*, vol. 4, n. 5, p. 1165-1185.
[3] Allix, O. and Ladevèze, P. (1992), *Composite structures*, vol. 22, n. 4, p. 235-242.
[4] Schellekens, J. C. J. and De Borst, R. (1993), *International Journal of Solids and Structures*, vol. 30, n. 9, p. 1239-12
[5] Cui, W., & Wisnom, M. R. (1993), *Composites*, vol. 24, n. 6, p. 467-474.
[6] Corigliano, A. (1993), *International Journal of Solids and Structures*, vol. 30, n. 20, p. 2779-2811
[7] Burda, I., Barbezat, M. and Brunner, A. J. (2020), *Fatigue & Fracture of Engineering Materials & Structures*, vol. 43, n. 2, p. 292-307.
[8] ASTM International D5528-13 (2013), *Standard Test Method for Mode I Interlaminar Fracture Toughness of Unidirectional Fiber-Reinforced Polymer Matrix Composites*, ASTM International, West Conshohocken.
[9] Mall, S. (1985), *Characterization of mode 1 and mixed-mode failure of adhesive bonds between composite adherends*. NASA, Langley Research Center.
[10] Airoldi, A. and Dávila, C. G. (2012), *Composite Structures*, vol. 94, n. 11, p. 3240-3249.
[11] Maire, J. F. and Chaboche, J. L. (1997), *Aerospace Science and Technology*, vol. 1, n. 4, p. 247-257.
[12] Simo, J. C. and Ju, J. (1987), *International journal of solids and structures*, vol. 23, vol. 7, p. 821-840.
[13] Williams, K. V., Vaziri, R. and Poursartip, A. (2003), *International Journal of Solids and Structures*, vol. 40, n. 9, p. 2267-2300.
[14] Ladeveze, P. and LeDantec, E. (1992), *Composites science and technology*, vol. 43, n. 3, p. 257-267.
[15] Ladevèze, P., Allix, O., Deü, J. F. and Lévêque, D. (2000). *Computer methods in applied mechanics and engineering*, vol. 183, n. 1-2, p. 105-122.
[16] Ladevéze, P. and Lubineau, G. (2001), *Composites Science and Technology*, vol. 61, n. 15, p. 2149-2158.
[17] Ladeveze, P. and Lubineau, G. (2002), *Composites Science and Technology*, vol. 62, n. 4, p. 533-541.
[18] Maimí, P., Camanho, P. P., Mayugo, J. A. and Dávila, C. G. (2007), *Mechanics of materials*, vol. 39, n. 10, p. 897-908.
[19] Maimí, P., Camanho, P. P., Mayugo, J. A. and Dávila, C. G. (2007), *Mechanics of materials*, vol. 39, n. 10, p. 909-919.
[20] Lubineau, G. and Ladevèze, P. (2008), *Computational Materials Science*, vol. 43, n. 1, p. 137-145.
[21] Maimi, P., Mayugo, J. A. and Camanho, P. P. (2008), *Journal of Composite Materials*, vol. 42, n. 25, p. 2717-2745.
[22] Abisset, E., Daghia, F. and Ladevèze, P. (2011), *Composites Part A: Applied Science and Manufacturing*, vol. 42, n. 10, p. 1515-1524.
[23] Johnson, A. F. (2001), *Composites Part A: Applied Science and Manufacturing*,vol. 32, n. 9, p. 1197-1206.
[24] Laws, N., Dvorak, G. J. and Hejazi, M. (1983), *Mechanics of Materials*, vol. 2, n. 2, p. 123-137.
[25] Dvorak, G. J., Laws, N. and Hejazi, M. (1985), *Journal of Composite Materials*, vol. 19, n. 3, p. 216-234.
[26] Dvorak, G. J. and Laws, N. (1987), *Journal of composite materials*, vol. 21, n. 4, p. 309-329.
[27] Hashin, Z. (1985), *Mechanics of materials*, vol. 4, n. 2, p. 121-136..
[28] Garrett, K. W. and Bailey, J. E. (1977), *Journal of materials science*, vol. 12, p. 157-168.
[29] Parvizi, A., Garrett, K. W. and Bailey, J. E. (1978), *Journal of Materials Science*, vol.13, p. 195-201.
[30] Parvizi, A. and Bailey, J. E. (1978), *Journal of Materials Science*, vol. 13, p. 2131-2136.
[31] Bader, M. G. (1979), In: *Proc. 3rd Intern. Conf.*, Cambridge, England, p. 227-239.
[32] Bailey, J. E., Curtis, P. T. and Parvizi, A. (1979). *Proceedings of the Royal Society of London. A. Mathematical and Physical Sciences*, vol. 366, n. 1727, p. 599-623.
[33] Manders, P. W., Chou, T. W., Jones, F. R. and Rock, J. W. (1983), *Journal of Materials Science*, vol. 18, p. 2876-2889.

[34] Fukunaga, H., Chou, T. W., Peters, P. W. M. and Schulte, K. (1984), *Journal of composite materials*, vol. 18, n. 4, p. 339-356.
[35] Wang, A. S. D. and Crossman, F. W. (1980), *Journal of Composite Materials*, vol. 14, n. 1, p. 71-87.
[36] Laws, N. and Dvorak, G. J. (1988), *Journal of composite materials*, vol. 22, n. 10, p. 900-916.
[37] Hallett, S. R., Jiang, W. G., Khan, B. and Wisnom, M. R. (2008), *Composites Science and Technology*, vol. 68, n. 1, p. 80-89.
[38] Berthelot, J. M. and Le Corre, J. F. (2000), *Composites Science and Technology*, vol. 60, n. 7, p. 1055-1066..
[39] Berthelot, J. M. and Le Corre, J. F. (2000), *Composites Science and Technology*, vol. 60, n. 14, p. 2659-2669.
[40] Berthelot, J. M. (2003), *Appl. Mech. Rev.*, vol. 56, n. 1, p. 111-147.
[41] Wisnom, M. R. and Hallett, S. R. (2009), *Composites Part A: Applied Science and Manufacturing*, vol. 40, n. 4, p. 335-342.
[42] Abisset, E., Daghia, F., Sun, X. C., Wisnom, M. R. and Hallett, S. R. (2016), *Composite Structures*, vol. 136, p. 712-726.
[43] Camanho, P. (2015), In: *Numerical modelling of failure in advanced composite materials*. Woodhead Publishing., Hallett, S. (Ed.)
[44] Reifsnider, K. (1980), *International Journal of Fracture*, vol 16, p. 563-583.
[45] van der Meer, F. P. and Dávila, C. G. (2013), *International Journal of Solids and Structures*, vol. 50, n. 20-21, p. 3308-3318.
[46] Iarve, E. V. (2003), *International Journal for Numerical Methods in Engineering*, vol. 56, n. 6, p. 869-882.
[47] Shi, Y. and Soutis, C. (2016), *Theoretical and Applied Fracture Mechanics*, vol. 83, p. 73-81.
[48] Mohammadi, B., Olia, H. and Hosseini-Toudeshky, H. (2015), *Composite Structures*, vol. 120, p. 519-530.
[49] Airoldi, A., Mirani, C. and Principito, L. (2020), *Composite Structures*, vol. 234, p. 111747.
[50] Airoldi, A., Baldi, A., Mostosi, V. and Sala, G. (2012), In: *Proceedings of the 15th European Conference on Composite Materials*, p. 1-8.
[51] Airoldi, A., Baldi, A., Bettini, P. and Sala, G. (2015), *Composites Part B: Engineering*, vol. 72, p. 137-149.
[52] Airoldi, A., Novembre E., Mirani C., Gianotti G. Passoni R., Cantoni C., (2023), *Materials Today Communication*, vol 35, 106059
[53] Camanho, P. P., Davila, C. G. and De Moura, M. F. (2003), *Journal of composite materials*, vol. 37, n. 16, p. 1415-1438.
[54] Hagenbeck M., (2005), In: *Characterisation of Fibre Metal Laminates under Thermo-mechanical Loadings*, PhD thesis, TUDelft